Resistivity, Hysteresis, and Magnetization of 9% Cr Stainless Steel as a Function of Temperature and Its Electromagnetic Shielding Effects in Cylindrical Structures*

W. F. Praeg
Argonne National Laboratory
Argonne, IL 60439

Summary

Ferromagnetic stainless steels may offer significantly greater wall life-times for first wall/blanket and vacuum vessel structures than commonly used non-magnetic stainless steels. One steel under consideration has the following composition, in weight percent,

Fe	Cr	Mo	Mn	Si	Nb	V	C	P	S
86.24	9.0	2.0	1.0	0.75	0.50	0.30	0.15	0.3	0.30

There appears to be no literature on the electromagnetic properties of this material. Therefore, the resistivity, the hysteresis loops, and magnetization were measured as a function of temperature up to the Curie point.

For Tokamak applications it is of specific interest to know the resistivity and saturation flux density in the range from 400 to 600°C. By applying a toroidal field that saturates the ferromagnetic steel, the first wall/blanket and vacuum vessel structures should respond to a superimposed alternating field like non-magnetic stainless steel. The field of the equilibrium coils, which gives the fine control of the position and shape of the plasma, must penetrate the first wall/blanket and/or vacuum vessel. Normalized graphs are given for the logarithmic ratio of external to internal alternating fields (shielding) as a function of the ratio of wall thickness to skin depth, with vessel radius, wall thickness, and permeability as parameters. These graphs should be useful for the design of feedback loops for equilibrium-field-coil power supplies and in the designing of electromagnetic shields with this material, either dc saturated or not.

Resistivity

A 300 cm long wire sample was drawn to a diameter of 0.159 cm and annealed at 1100°C for half an hour. The resistance of the sample was measured with a Kelvin bridge at temperatures ranging from -195.8°C (liquid nitrogen) to 800°C. Figure 1 shows the resistivity calculated from these measurements. When the resistivity was calculated, no corrections were made to account for the effects of the coefficient of thermal expansion of the material. For comparison, the commonly known resistivity of Types 304 and 316 stainless steel is also shown.

Permeameter Measurements

A sample of material was machined to the dimensions 1.232 x 1.232 x 2.540 cm, and the B-H curves shown in Figs. 2 and 3 were measured with a permeameter at the Arnold Engineering Co. in Marengo, IL. This permeameter uses a large electromagnet to generate magnetic fields of up to 16 x 10^3 Oe in the tips of large pole pieces shaped like the frustum of a circular cone. The distance between the pole pieces is adjustable to accommodate samples of different lengths. A very thin wire is taped around the middle of the sample to serve as a one turn B coil. The magnetic field H is measured with a Hall plate. The B-coil signal is amplified and integrated and used for the vertical deflection of a

*Work supported by the U.S. Department of Energy

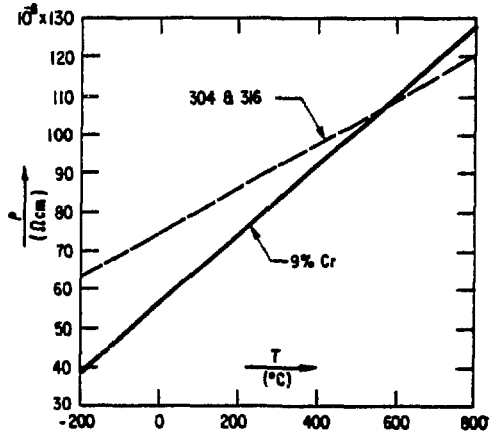

Figure 1 Electrical Resistivity in Stainless Steels

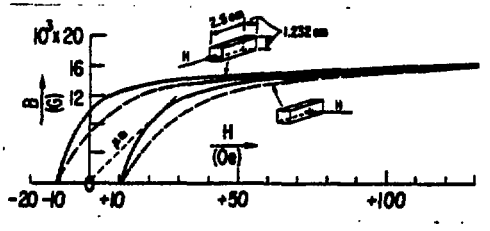

Figure 2 DC Hysteresis Loops of 9% Cr Stainless Steel Sample for H ≤ 130 Oe

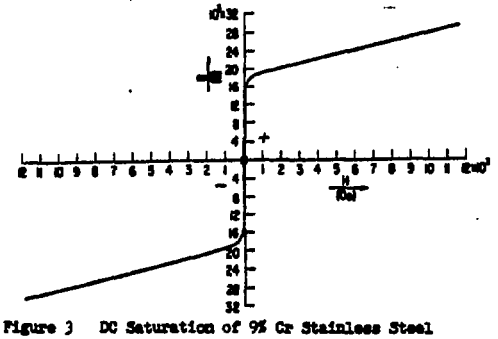

Figure 3 DC Saturation of 9% Cr Stainless Steel

recorder. The amplified H signal is used for the horizontal deflection of the recorder. From Fig. 2 the steel appears to be isotropic having a maximum permeability of $\mu_m \approx 400$ at 10 kG. The two solid curves were measured when the sample was energized in the direction of its 2.540 cm axis. The two dashed curves were measured when the sample was energized in the direction of a 1.232 cm axis. In the permeameter the ratio of the length of the air gap ℓ_{air} to the length of the iron sample ℓ_{Fe} is larger when the sample is magnetized along a 1.232 cm axis as compared to magnetizing along the 2.54 cm axis; this larger ratio of ℓ_{air}/ℓ_{Fe} causes the slope of the dashed curve to be smaller as compared to the slope of the solid curve. From Figs. 2 and 3 we see that the steel saturates at room temperature at $\leq$ 20 kG.

Measurements on a Toroidal Sample

Sample Preparation

A toroidal sample was machined to an outside diameter of 10.16 cm and a cross section of 1.11 x 1.11 cm and its dimensions measured with an accuracy of ±0.0025 cm. A 0.01 cm thick coating of aluminum oxide was plasma-sprayed on the toroid for insulation. Next a B coil was wound on the core by uniformly spacing 103 turns of No. 26 AWG Nichrome wire. The B coil was covered with high-temperature ceramic cement (SAUEREISEN No. 6). An excitation coil of 354 turns of bare No. 18 AWG copper wire was wound over the B coil in three layers. Ceramic cement was applied after each layer and the assembly was baked in an oven. Turn-to-turn insulation was provided by placing a glass-quartz string of 0.1 cm diameter between turns.

Measuring Circuits

Temperature. A nickel-chromium versus nickel-aluminum (Chromel-Alumel) thermocouple was imbedded in a small hole drilled 2.5 cm deep into a piece of steel 1.11 x 1.11 x 5 cm. The steel was then covered with the same thickness of cement as the toroid and placed in the oven next to the toroid. Two more thermocouples were placed in the center of the toroid. Inside the oven, the wires of the three thermocouples were insulated with ceramic tubing. Outside the oven, each thermocouple was connected to a similar thermocouple in series opposition. In this way the thermocouple effects of the interconnections at room temperature between the millivolt meter and the thermocouples cancel. The number of millivolts produced is the difference in millivolts between the temperature of the thermocouple in the oven and the temperature of the thermocouple on the outside. The three outside thermocouples were placed in an agitated ice bath; in this way the oven temperatures were measured with reference to 0°C. The thermocouple voltages were monitored with a Fluke digital voltmeter Model No. 8600 A. The thermocouple temperature was read with an accuracy of ±0.2%.

Magnetizing Force H and Induction B. The toroid was excited with a 0.5 Hz sinusoidal current (sin ωt = sin πt). The current was monitored by measuring the voltage drop on a noninductive resistor of 0.340 Ω. By means of a stable amplifier, the voltage on the resistor was amplified to produce on the screen of an oscilloscope a horizontal peak-to-peak deflection of ten divisions. The oscilloscope was a Tektronix Model 706 with a Model 7A13 time base. The voltage induced in the B coil was fed to an electronic integrator to obtain $\int \dot{B}\,dt = B$. The B signal was used for the vertical deflection of the scope. The integrator has a time constant of 50 s. The flux-meter installation was calibrated with a square-wave signal to an accuracy of ±2%.

Measurements

Hysteresis Loops. A magnetization curve (solid) and a hysteresis loop (dotted) together with some important magnetic quantities are shown for definition in Fig. 4. Figure 5 shows a few of the hysteresis loops measured. In these pictures, the excitation is held constant at $H = H_0 \sin \omega t = 55 \sin \pi t$ Oe and the temperature T is changed. The oven has a regulator that holds temperature within a few degrees of a set point. It took approximately two hours at a set point to reach a stable temperature in the toroid. The sensitivity of the B scale was increased to take measurements near the Curie point; this is illustrated by Fig. 6. The results of the measurements are summarized in Figs. 7 and 8. Referring to Fig. 7, the Curie point of the sample is at 705°C ± 4°C. Its maximum permeability $\mu_m = 675$ is reached around 400°C. At 20°C we have $\mu_m \approx 515$; this is larger than the $\mu_m \approx 400$ shown in Fig. 2. The difference is due to the unavoidable air gaps when measuring with the permeameter. The air gaps cause a smaller slope (shearing) of the B-H curve.

The coercive force, Hc, declines as the temperature increases. At room temperature the value measured with the permeameter is $H_c = 11$ Oe. The value measured with 0.5 Hz applied to the toroid is $H_c = 12.4$ Oe. The difference is due to an increase in eddy-current losses at 0.5 Hz as compared to the slower changes of dH/dt with the permeater measurements. At 20°C the 0.5 Hz skin depth

$$\delta = \left(\frac{\rho}{\mu \pi f}\right)^{1/2} \qquad (1)$$

of the toroid material is

$$\delta = \left(\frac{77.3\ \mu\Omega\ \text{cm}}{0.4\pi \times 10^{-8}\ \Omega\ \text{s/cm} \times 515 \times \pi \times 0.5\ \text{s}^{-1}}\right)^{1/2}$$

$$= 2.37\ \text{cm},$$

which is 4.3 times the half-thickness of the toroid. Figure 9 shows the effect of frequency on the hysteresis loop of the toroid. At 20°C ($\delta = 2.37$ cm) the loop widens noticeably between 0.05 Hz (~ dc case) and 0.5 Hz. From Fig. 9 the dc permeability can be calculated as $\mu_m \approx 870$, which is 69% larger than the 0.5 Hz permeability of $\mu_m = 515$ shown in Fig. 7. Above 600°C with $\delta \geq 3.48$ cm, the effect of frequency is smaller and disappears as we get closer to the Curie point. Also shown in Fig. 7 is the permeability at 55 Oe, μ_{55Oe}, as a function of temperature. Figure 8 shows the induction at 55 Oe, B_{55Oe}, and the residual induction, B_r, versus temperature. The induction at maximum permeability, μ_m, has nearly the same values as B_r.

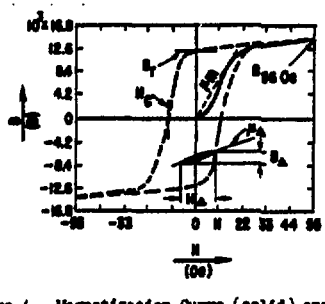

Figure 4 Magnetization Curve (solid) and Hysteresis Loop (dotted)

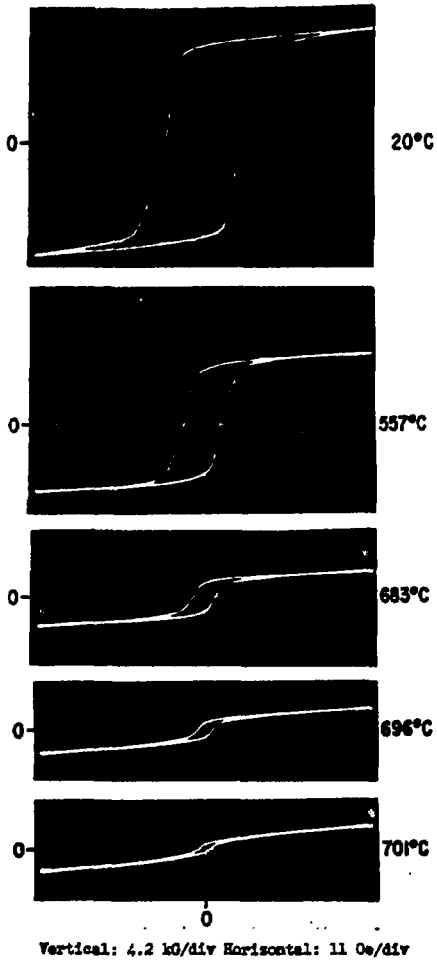

Vertical: 4.2 kG/div Horizontal: 11 Oe/div

Figure 5 Hysteresis Loops at Various Temperatures for H = 55 sin wt Oe

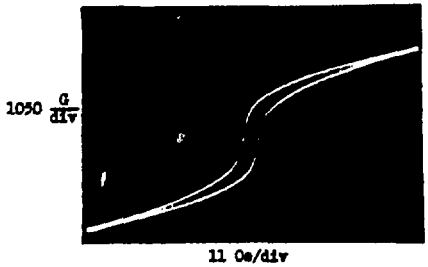

11 Oe/div

Figure 6 Hysteresis Loop at 696°C

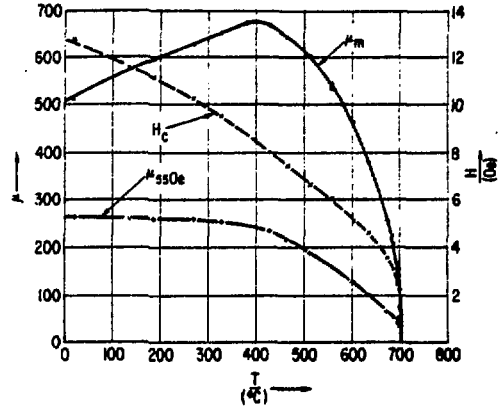

Figure 7 Variation of Permeability and Coercive Force With Temperature for H = 55 sin wt Oe

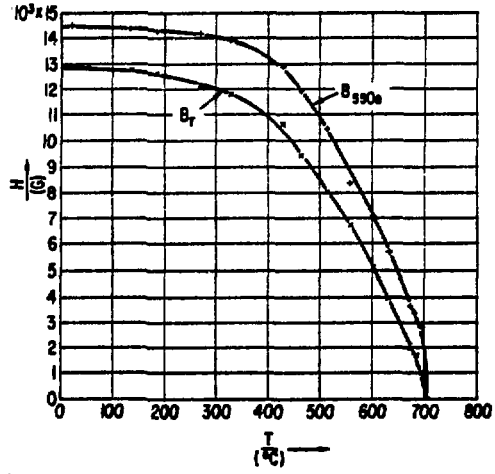

Figure 8 Variation of B_{550e} and B_r With Temperature for H = 55 sin wt Oe

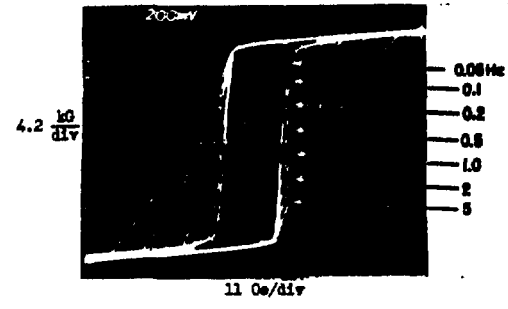

11 Oe/div

Figure 9 Hysteresis Loops of Toroidal Sample for Various Frequencies at 20°C

Magnetization. Magnetization curves, measured at room temperature and at 600°C are shown in Fig. 10. To plot these curves, pictures were taken with magnetizing forces of $H \geq 1$ Oe after the toroid had been demagnetized by heating it above the Curie point. Figures 11 and 12 show composites of different hysteresis loops taken at 20 and 600°C, respectively. The tips of these loops lie on the respective magnetization curves.

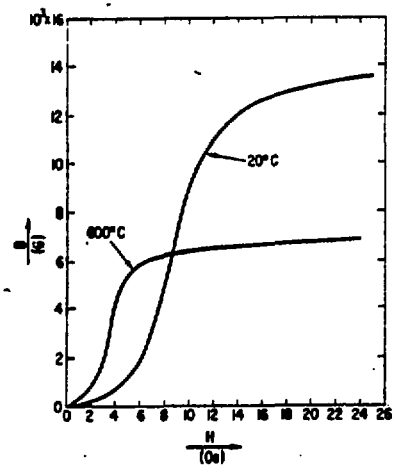

Figure 10 Magnetization Curves at 20°C and 600°C

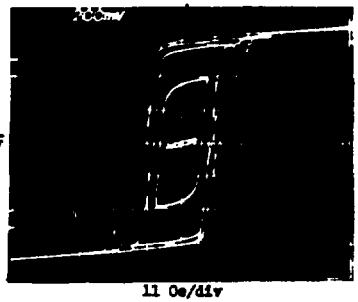

Figure 11 Hysteresis Loops at 20°C for Various Magnitudes of Field Strength

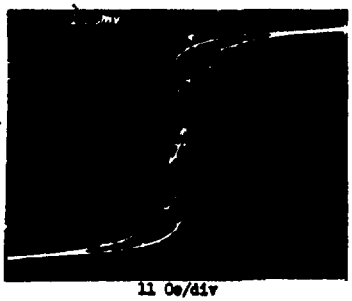

Figure 12 Hysteresis Loops at 600°C for Various Magnitudes of Field Strength

Electromagnetic Shielding

In a Tokamak the field of the equilibrium coils, which gives the fine control of the position and shape of the plasma, must penetrate the first wall and/or the vacuum vessel.

With the resistivity, ρ, and the permeability, μ, known, we can calculate the electromagnetic shielding effects of cylindrical structures built from 9% Cr steel. Two conditions are considered. First, the toroidal field is assumed to saturate the cylinder along its axis. At room temperature, toroidal fields of ≥ 20 kG and at 500°C fields of ≥ 16 kG completely saturate the steel (see Figs. 3 and 8). The equilibrium field, which is transverse to the axis of the cylinder, causes only rotations of the saturated domains in the steel.[2] The incremental permeability is $\mu_\Delta = B_\Delta/B_\Delta = 1$ G/Oe. This is the same as a nonmagnetic cylinder. Second, for completeness sake we also consider applications in which the 9% Cr steel is used unsaturated as an electromagnetic cylindrical shield.

As shown in Fig. 13, a homogeneous alternating field H_o (the field of the equilibrium coils) is applied transverse to the axis of the cylinder; the resulting electric field E is in the direction of the cylinder axis Z. The field inside the cylinder H_i can be written

$$\left.\begin{aligned} H_r &= H_i \sin\Psi = Q H_o \sin\Psi \\ H_\Psi &= H_i \cos\Psi = Q H_o \cos\Psi \end{aligned}\right\} \quad o \leq r \leq r_o \qquad (2)$$

The factor of electromagnetic shielding Q can be written[1]

$$Q = \frac{H_i}{H_o} = \frac{1}{\cosh kd + \frac{1}{2}(K + \frac{1}{K}) \sinh kd} \qquad (3)$$

where

k = eddy current constant $= \frac{1+j}{\delta}$,

$j = (-1)^{1/2}$,

δ = skin depth $= \left(\frac{\rho}{\mu\pi f}\right)^{1/2}$,

$K = \frac{\mu_o}{\mu} k r_o$,

$\mu_o = 0.4\pi \times 10^{-8} \frac{H}{cm}$ permeability of space,

and

μ = permeability.

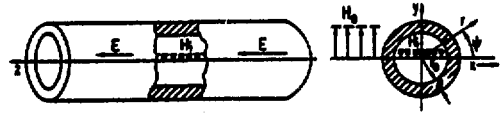

Figure 13 Cylinder in an Alternating Field H_o Transverse to its Axis Z

Nonmagnetic Cylinder. With the cylinder saturated ($\mu_\Delta = \mu_0$), $|K| = |k\, r_0| \gg 1$, the term 1/K in Eq. (3) can be neglected, and we have for the shielding factor

$$Q = \frac{1}{\cosh kd + \frac{1}{2} K \sinh kd}. \qquad (3')$$

The attenuation a_s of the cylinder is defined by

$$a_s = \ln \frac{1}{|Q|} = \ln \left|\frac{H_o}{H_i}\right| \qquad (4)$$

From Eqs. (3' and 4), we obtain

$$a_s = \ln \frac{1}{|Q|} = \frac{1}{2} \ln \left[\left(\frac{r_o}{2\delta}\right)^2 \left(\cosh \frac{2d}{\delta} - \cos \frac{2d}{\delta}\right) + \frac{r_o}{2\delta}\left(\sinh \frac{2d}{\delta} - \sin \frac{2d}{\delta}\right) + \frac{1}{2}\left(\cosh \frac{2d}{\delta} + \cos \frac{2d}{\delta}\right)\right]. \qquad (5)$$

Figure 14 shows the attenuation, calculated from Eq. (5), as a function of d/δ, which is proportional to the square root of the frequency, for different parameters $p = r_o/2d$. For low frequencies (d < δ) and for high frequencies (d > δ), Eq. (5) can be simplified to

$$a_s = \ln \frac{1}{|Q|} = \frac{1}{2} \ln \left[1 + \left(\frac{r_o}{\delta^2} \frac{d}{2}\right)^2\right] \quad \text{for } d < \delta, \qquad (6)$$

$$a_s = \ln \frac{1}{|Q|} = \frac{d}{\delta} + \ln \frac{r_o}{2\sqrt{2}\,\delta} \quad \text{for } d > \delta. \qquad (7)$$

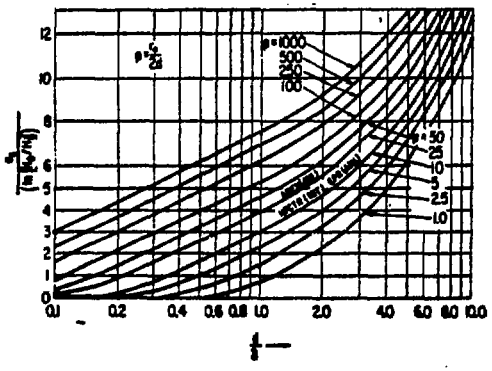

Figure 14 Attenuation a_s of a Nonmagnetic Cylinder

Examples of Shielding Effects. The vacuum vessel of Argonne's APEX Tokamak is made from Type 304 stainless steel (ρ = 74 μΩ cm at 20°C). It has a radius of 15.2 cm and a wall 0.30 cm thick. For frequencies of 1 and 10 kHz, we have δ = 1.36 and δ = 0.43 respectively, resulting in ratios of d/δ = 0.22 and 0.70. From Eqs. (5-7), or from Fig. 14, we find an attenuation of $a_s = \ln |H_o/H_i| = 0.93$ at 1 kHz and $a_s = 3.23$ at 10 kHz. This corresponds to field ratios $|H_o/H_i|$ of 2.59 and 25.3 respectively.

Argonne's EPR design has a 7 cm thick vacuum vessel made from Type 316 stainless steel. With an average radius of $r_o \approx 220$, we have $p = r_o/2d = 15.7$. Operating at 400°C we find from Fig. 1 a resistivity ρ = 98 μΩ cm. For frequencies of 10 and 100 Hz, we have d/δ = 0.444 and 1.41, respectively. From Eq. (5) or the curves of Fig. 14 we find for 10 Hz an attenuation $a_s = \ln |H_o/H_i| = 1.84$ and for 100 Hz, $a_s = 4.16$. This corresponds to ratios of $|H_o/H_i| = 6.3$ and 64, respectively. A total of 20 cm of stainless steel first wall/blanket material is inside the vacuum vessel to minimize radiation damage to the vessel. If this 20 cm thick material were also in the form of a vessel the combined wall thickness would be d ≈ 27 cm. For frequencies of 10 and 100 Hz we would have d/δ = 1.71 and 5.42, respectively. From Eq. (7) the attenuation at 10 Hz would be $a_s = 3.31$ and at 100 Hz, $a_s = 8.17$. This corresponds to ratios of $|H_o/H_i| = 27.5$ and 3533, respectively. In order to reduce eddy-current shielding the first wall/blanket is made from 128 blocks which are insulated from each other. Each block is made from a 20 cm thick Type 316 stainless steel flat plate.

Magnetic Cylinders. With $\mu \gg \mu_o$, the value of 1/K in Eq. (3) is larger than 1 and can no longer be neglected. From Eqs. (3 and 4), the general equation for the attenuation is given by[1]

$$a_s = \ln \frac{1}{|Q|} = \frac{1}{2} \ln \left[\left(\frac{\mu_o r_o}{2\mu d}\right)^2 + \left(\frac{\mu\delta}{4\mu_o r_o}\right)^2\right] \times \left(\cosh \frac{2d}{\delta} - \cos \frac{2d}{\delta}\right) + \frac{\mu_o r_o}{2\mu\delta}\left(\sinh \frac{2d}{\delta} - \sin \frac{2d}{\delta}\right) + \frac{\mu\delta}{4\mu_o r_o}\left(\sinh \frac{2d}{\delta} + \sin \frac{2d}{\delta}\right) + \frac{1}{2}\left(\cosh \frac{2d}{\delta} + \cos \frac{2d}{\delta}\right)\Bigg] \qquad (8)$$

Figure 15 shows the attenuation as a function of d/δ for various values of the parameter $p = \mu_o r_o/\mu d$. The difference of these curves as compared to the curves of Fig. 14 is that, at low frequencies, all curves have constant values. These values represent the magnetostatic shielding of the cylinders. At the limit with δ → ∞ (or f → 0), Eq. (8) reduces to

$$\lim_{\delta \to \infty} a_s = \ln\left(1 + \frac{1}{2} \frac{\mu d}{\mu_o r_o}\right) \qquad (9)$$

At very high frequencies, where $\mu_o r_o/\mu\delta \gg 1$, the field does not penetrate the cylinder appreciably and magnetostatic effects disappear. In this case Eq. (8) reduces to Eq. (5).

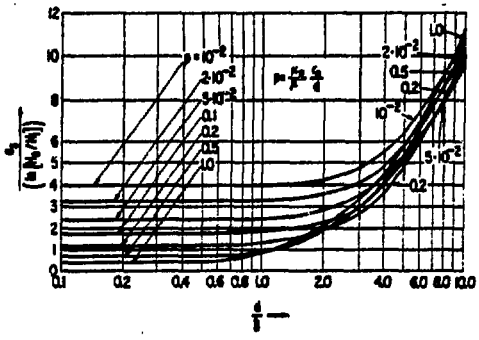

Figure 15 Attenuation a_s of a Magnetic Cylinder

Acknowledgement

It is a pleasure to acknowledge the support of Don McGhee who designed and built the integrator and amplifier circuits and patiently took over 100 oscilloscope pictures.

References

1. H. Kaden, "Wirbelströme und Schirmung in der Nachrichtentechnik," Springer-Verlag, Berlin, 1959.
2. R. M. Bozorth, "Ferromagnetism," D. Van Nostrand Co. Inc., New York, 1959.